

Parameter Identification of a Differentiable Human Arm Musculoskeletal Model without Deep Muscle EMG Reconstruction

Philip Sanderink, Yingfan Zhou, Shuzhen Luo, Cheng Fang

Abstract— Accurate parameter identification of a subject-specific human musculoskeletal model is crucial to the development of safe and reliable physically collaborative robotic systems, for instance, assistive exoskeletons. Electromyography (EMG)-based parameter identification methods have demonstrated promising performance for personalized musculoskeletal modeling, whereas their applicability is limited by the difficulty of measuring deep muscle EMGs invasively. Although several strategies have been proposed to reconstruct deep muscle EMGs or activations for parameter identification, their reliability and robustness are limited by assumptions about the deep muscle behavior. In this work, we proposed an approach to simultaneously identify the bone and superficial muscle parameters of a human arm musculoskeletal model without reconstructing the deep muscle EMGs. This is achieved by only using the least-squares solution of the deep muscle forces to calculate a loss gradient with respect to the model parameters for identifying them in a framework of differentiable optimization. The results of extensive comparative simulations manifested that our proposed method can achieve comparable estimation accuracy compared to a similar method, but with all the muscle EMGs available.

I. INTRODUCTION

In recent years, a variety of robots have gradually been integrated into human work and daily life. For better safety and performance, human musculoskeletal modeling, as an essential component, has also been actively incorporated into diverse physical human-robot interaction scenarios like ergonomic co-manipulation with collaborative robots, rehabilitation therapy planning with assistive exoskeleton devices, and the restoration of mobility with powered prosthetic limbs [1]–[4]. Reactions to the same robot behavior may vary across different individuals. Personalizing a human musculoskeletal model by identifying individualized model parameters is the first crucial step in simulating subject-specific dynamic behavior in a simulator, which facilitates the design of a robot controller prior to real-world implementation. In addition, accurate estimation of subject-specific parameters can also enable convenient evaluation of muscle and tendon quality, such as, muscle strength and tendon stiffness, with wide applications across sports science, rehabilitation engineering, and medical diagnostics [5]–[7].

Typically, a subject-specific musculoskeletal model is built by scaling a template model, with base parameters obtained or estimated from cadaver-based statistical datasets representing a given population [8]. The scaling factors are calculated based on the recorded motion data of an individual and they are used to scale both bone dynamic parameters and muscle parameters. Although it has been widely demonstrated that the inaccuracy of bone parameter estimates has a lesser

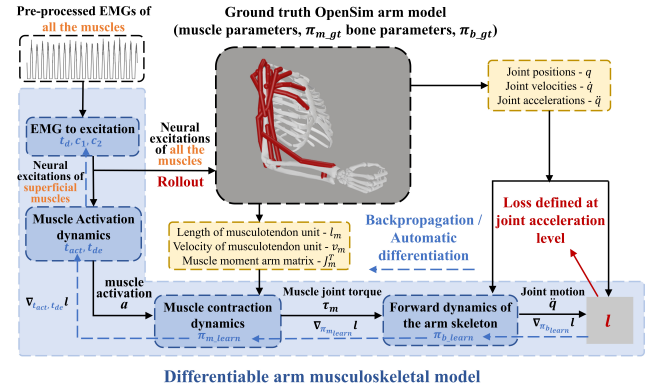


Fig. 1: A differentiable human arm musculoskeletal model for simultaneous identification of the bone and muscle parameters without deep muscle EMG reconstruction.

impact on the inaccuracy of dynamic behavior than the inaccuracy of kinematic parameters [9], the muscle parameters do have a significant effect [10], [11]. To improve muscle parameter estimation, individual EMG signals can be utilized [12], [13]. Well-preprocessed EMGs can be used to drive a musculoskeletal model to calculate the joint torque and the resulting motion, which can be used to compute a loss by comparing it against the observed motion. The muscle and bone parameters can thus be estimated by solving a non-linear optimization problem that minimizes the loss [14]–[17]. However, activities of superficial muscles can be easily measured by surface EMG sensors, whereas those of deep muscles cannot [18]. In practice, deep muscles can be measured using fine-wire electrodes, but such measurements are invasive and require specialized expertise; therefore, they are impractical for daily use or large-scale applications [19]. Such a limitation raises a question: *Can some of the musculoskeletal model parameters still be identified without access to the EMG recordings of deep muscles?*

This research makes two primary contributions:

- 1) We propose simultaneously identifying the superficial muscle and bone parameters of a human arm musculoskeletal model without reconstruction of deep muscle EMG signals using differentiable optimization for the first time.
- 2) We present extensive simulations with a high-fidelity human arm musculoskeletal model (11 superficial muscles and 5 deep muscles) that demonstrate our proposed approach can achieve good estimation results.

II. RELATED WORKS

EMG-based musculoskeletal modeling approach has been widely employed for musculoskeletal model calibration

to identify muscle parameters (e.g., optimal fiber length and maximum isometric force) and/or rigid bone dynamic parameters (e.g., mass and center of mass). The parameter estimation is typically formulated as an optimization problem with a loss function defined either at the joint torque or joint acceleration level. If the experimental EMG data of all the muscles of interest can be obtained, and skeletal dynamic parameters are available, either from statistical mass distribution models [20] or from scaling techniques driven by kinematic data [21], internal joint torques can be derived through inverse dynamics of the rigid skeleton with measured motion as the inputs. Then, muscle parameters can be estimated by solving the optimization problem with the loss defined between the derived joint torques and the predicted ones calculated from muscle activation and contraction dynamics models with the neural excitations as the input obtained from processed EMG recordings [14]–[17]. Due to the strong non-linearity and non-convexity inherent in muscle dynamics, this optimization problem is typically addressed through global optimization algorithms, such as simulated annealing [22] or particle swarm algorithms [23]. However, any inaccuracies of the bone parameter estimates would propagate to the calculated joint torques and ultimately compromise the accuracy of the identified muscle parameters [24]. To tackle this issue, a differential musculoskeletal model was proposed to simultaneously estimate the muscle and bone parameters, which demonstrated better results against the global optimization methods in a simulation study [17].

However, in real experiments, it is not practical to easily acquire EMG signals from deep muscles. To cope with this limitation, the EMG-assisted strategy allows for synthesizing unmeasurable muscle EMG signals and, meanwhile, adjusting recorded observable EMG signals to reduce the discrepancy between the predicted joint torques and the measured ones [25]. However, introducing synthesized or altered EMG signals into the calibration may compromise its fidelity and yield physiologically unreliable estimates. Alternatively, muscle synergy extrapolation (MSE) has been also widely used to estimate EMG data from deep or missing muscles. Muscle synergy refers to the coordinated activation of groups of muscles that act together as functional units to produce movement [26]. With MSE, recorded surface EMG signals are projected onto a reduced subspace represented by time-varying synergy excitations as the basis functions and time-invariant weight vectors. The extracted basis synergy patterns are subsequently utilized to reconstruct the EMG activity of deep muscles, which, together with the measured EMG signals from surface muscles, are used to drive EMG-based musculoskeletal models for parameter identification [27]–[30]. In particular, principal component analysis and non-negative matrix factorization are the most widely adopted approaches for synergy extraction [31]. Although MSE strategy yields physiologically consistent muscle excitation reconstruction, the reliability of the reconstructed signals depends heavily on the specific extraction method employed and the number of synergies to be selected, which can substantially compromise the accuracy of deep muscle reconstruction and consequen-

tly hinder the reliable identification of model parameters [32]. In recent years, advances in deep neural networks have introduced new perspectives for EMG-based parameter identification. Particularly, physics-informed neural networks enhance musculoskeletal model parameter identification by embedding a physics-based model into a data-driven learning paradigm, thereby improving interpretability and accuracy for parameter identification even with limited or unlabeled data [33]–[35]. Recently, to address the problem of the lack of deep muscle EMGs, a neural network-based musculoskeletal model was proposed to reconstruct deep muscle EMGs from motion data while integrating surface EMGs to ensure physiological consistency and simultaneously enable musculoskeletal parameter identification [36]. However, the identified parameters were not tested in new datasets with movement and conditions different from the training data.

III. OUR APPROACH

Since the invasive and accurate reconstruction of the deep muscle EMGs is difficult and different combinations of EMGs might generate the same observed movement (redundancy in the muscle recruitment), we propose to identify the model parameters of a human arm musculoskeletal model without the EMG reconstruction of the deep unmeasurable muscles.

A. Differentiable optimization

There is an emerging paradigm of solving the parameter estimation in sim-2-real gap [37]–[39] in robotics by using differential optimization/simulation [40], [41], where the gradients of the loss relative to the model parameters are computed by automatic differentiation [42] on a computational graph reflecting the topological dependency between a large number of intermediate variables and parameters of a model, and the gradients are used to minimize the loss to find the optimal model parameters. The power of the differentiable optimization for simultaneously identifying a large number of bone and muscle parameters of a musculoskeletal model has been demonstrated in [17] recently.

B. Differentiable arm musculoskeletal model

To have better model realism as preparation for the future real experiments, an OpenSim human arm musculoskeletal model, “*MoBL-ARMS Dynamic Upper Limb*” [43], instead of a simplified MyoSuite model (used in [17]), is adopted as a reference model to generate ground truth training data. A differentiable version of this OpenSim model is developed outside the OpenSim to carry out the differentiable optimization (shown in Fig. 1) where the bone and muscle parameters are allowed to be changed and optimized to minimize a loss (error) of a variable, e.g., joint acceleration. In our differentiable arm model, the shoulder and elbow joints are movable while the wrist and finger joints are locked. The shoulder consists of three independent joint Degrees of Freedom (DoFs): flexion-extension (*Sh_Fle_Ext*), abduction-adduction (*Sh_Abd_Add*), and medial-lateral rotation (*Sh_Med_Lat*) DoFs, while the elbow is comprised of two independent joint DoFs: flexion-extension (*El_Fle_Ext*) and

pronation-supination (*El_Pro_Sup*) DoFs. The differentiable model includes eleven superficial muscles and five deep muscles, which are important for the movement generation of the shoulder and elbow joints. The superficial muscles include: the superior (*PECM1*), middle (*PECM2*), and inferior (*PECM3*) portions of the Pectoralis Major (Prime Mover, PM, of *Sh_Fle_Ext* and *Sh_Abd_Add*); the anterior (*DELT1*), lateral (*DELT2*), posterior (*DELT3*) portions of the Deltoid (PM of *Sh_Fle_Ext* and *Sh_Abd_Add*); the long (*BIClong*) and short portions (*BICshort*) of the Biceps (PM of *El_Fle_Ext*); the long (*TRIlong*) and lateral (*TRIlat*) portions of the Triceps (PM of *El_Fle_Ext*), and Brachioradialis (*BRD*). The deep muscles are: the Infraspinatus (*INFSP*, PM of *Sh_Med_Lat*), Subscapularis (*SUBSC*, PM of *Sh_Med_Lat*), the medial portion of the Triceps (*TRImed*, PM of *El_Fle_Ext*), Brachialis (*BRA*, PM of *El_Fle_Ext*), and the Pronator quadratus (*PQ*, PM of *El_Pro_Sup*) muscles [44].

In contrast to the differentiable arm model used in [17], to improve the realism of the model and make it ready for practical use in the real experiments, deep PM muscles are modeled but their EMGs are not assumed to be available, the EMG to muscle neural excitation dynamics and muscle activation dynamics are added, and constrained arm model is also considered in this work.

C. Constrained arm model

In the OpenSim model, there are eleven dependent DoFs whose values depend on the three independent DoFs of the shoulder joint. These dependencies are formulated as kinematic constraints in the dynamic system of the arm skeleton to incorporate, for instance, the effect of the topological loops created by sets of bones and joints. The constraints also introduce constraint torques to the equation of motion of the arm [45]:

$$M\ddot{q} + \tau_{bias} + G^T \lambda = J_m^T f_m, \quad (1)$$

$$G\ddot{q} = b, \quad (2)$$

where $M_{16 \times 16}$ is the inertia matrix, $\ddot{q}_{16 \times 1}$ denotes the accelerations of all the 16 independent and dependent joint DoFs, $\tau_{bias_{16 \times 1}}$ indicates the bias torque because of the Coriolis and centrifugal effects and the gravity. $G_{11 \times 16}$ and $b_{11 \times 1}$ in (2) are constant matrix and vector which are used to describe the constraints, and a vector of unknown Lagrange multipliers, $\lambda_{11 \times 1}$, is mapped to the constraint torques through G^T in (1). $f_{m_{16 \times 1}}$ means the forces produced by all the 16 muscles, and $J_{m_{16 \times 16}}$ is a muscle Jacobian, in which each element is a moment arm of a muscle with respect to a joint DoF calculated by the partial derivative of the length of a musculotendon unit relative to a DoF [46]. $J_m^T f_m$ represents the torques τ_m applied by all the muscles.

D. Addressing deep muscle behavior

Let's examine how the deep muscles would affect the dynamics of the arm skeleton, focusing on the five independent DoFs. The deep muscles, *INFSP* and *SUBSC*, span over the three DoFs of the shoulder, *TRImed* and *BRA* only affect the *EL_Fle_Ext* of the elbow, and *PQ* only causes joint torque

	PECM1	PECM2	PECM3	DELT1	DELT2	DELT3	BIClong	BICshort	TRIlong	TRIlat	BRD	INFSP	SUBSC	TRImed	BRA	PQ
Sh_Fle_Ext	r	r	r	r	r	r	r	r	r	0	0	r	r	0	0	0
Sh_Abd_Add	r	r	r	r	r	r	r	r	r	0	0	r	r	0	0	0
Sh_Med_Lat	r	r	r	r	r	r	r	r	r	0	0	r	r	0	0	0
El_Fle_Ext	0	0	0	0	0	0	r	r	r	r	r	0	0	r	r	0
El_Pro_Sup	0	0	0	0	0	0	r	r	0	0	r	0	0	0	0	r

Superficial Muscles

Deep Muscles

Fig. 2: Moment arms of different superficial and deep muscles of a human arm musculoskeletal model. *r* means a muscle spans over a joint and therefore has a moment arm with respect to the joint.

on the *EL_Pro_Sup* of the elbow throughout most of the range of motion. The contribution of the deep muscles to the joint torques can be described by the transpose of the deep muscle Jacobian, J_{md}^T ¹, shown on the right side of Fig. 2. It can be easily seen that the 3×2 non-zero muscle moment arm submatrix in the upper left corner of J_{md}^T renders an overdetermined system of linear equations in terms of the joint torques of the three shoulder DoFs which have to be provided by the *INFSP* and *SUBSC*, while the 2×3 moment arm submatrix in the lower right corner of J_{md}^T makes an underdetermined system of linear equations in terms of the required joint torques of the two elbow DoFs for the *TRImed*, *BRA*, and *PQ*. These two decoupled submatrices are the important matrix properties we will utilize to estimate the model parameters.

We propose to treat the deep muscle behavior as a black box, and only care about the output of the box, which is the muscle force f_m , without modeling the internal muscle dynamic behavior, i.e., without reconstructing the deep muscle EMGs or optimizing their muscle parameters. By virtue of the overdetermined system, all the bone parameters and the muscle model parameters of the muscles that would affect the three shoulder DoFs (i.e., the *PECM1*, *PECM2*, *PECM3*, *DELT1*, *DELT2*, *DELT3*, *BIClong*, *BICshort*, and *TRIlong* shown in Fig. 2) can be estimated if we define the loss as the error between the missing deep muscle torques and the provided torques calculated by the least-squares solution of the muscle forces of the the *INFSP* and *SUBSC*. This is because if the model parameter estimates are inaccurate, they would generate wrong missing deep muscle torques of the three shoulder DoFs, which cannot be perfectly compensated by the best possible solution of the deep muscle forces unless the estimates are at the ground truth. The residual torque error makes the gradient of the loss with respect to the model parameters non-zero, which can guide the optimization to find the right model parameters. On the other hand, due to the underdetermined system, the muscle parameters of the superficial muscles, which only affect the two elbow DoFs (i.e., *TRIlat* and *BRD* shown in Fig. 2) cannot be estimated because any missing wrong deep muscle torques of the two elbow DoFs caused by inaccurate muscle parameters can be always well compensated by infinite number of solutions of

¹The real dimension of J_{md}^T is 16×5 where the moment arms of the deep muscles over the 11 dependent DoFs are zeros. The dependent DoFs are ignored in Fig. 2 for better expression clarity.

the forces provided by the *TRImed*, *BRA*, and *PQ*. Therefore, the loss gradient would vanish.

E. Loss calculation

The loss caused by the proposed least-squares solution of the deep muscle forces can be calculated based on the constrained arm model ((1) and (2)) with known motion (q, \dot{q}, \ddot{q}) and estimated M and τ_{bias} . Let's assume,

$$\ddot{q} = \ddot{q}_u - \ddot{q}_c, \quad (3)$$

$$\ddot{q}_u = M^{-1}(\tau_m - \tau_{bias}), \quad (4)$$

where \ddot{q}_u and \ddot{q}_c are the joint accelerations of the corresponding unconstrained system and the offset caused by the constraints, respectively. Substituting (3) into (2), we have,

$$G\ddot{q}_c = G\ddot{q}_u - b. \quad (5)$$

In the meantime, after substituting (3) and (4) into (1), it can be seen that,

$$M\ddot{q}_c = G^T \lambda. \quad (6)$$

To solve for \ddot{q}_c with (5) alone, there exists an infinite number of solutions due to the underdetermined system in (5). However, the solution of \ddot{q}_c must be within the image space of $M^{-1}G^T$ shown in (6), therefore, a pseudoinverse with a weighting matrix of M must be used to solve for \ddot{q}_c :

$$\ddot{q}_c = G^{M+}(G\ddot{q}_u - b) = M^{-1}G^T(GM^{-1}G^T)^{-1}(G\ddot{q}_u - b), \quad (7)$$

where the invertibility of $GM^{-1}G^T$ is checked to ensure the existence of the weighted pseudoinverse for all the data points during the optimization. Accordingly, the Lagrange multiplier vector λ can be obtained with (6) and (7):

$$\lambda = (GM^{-1}G^T)^{-1}(G\ddot{q}_u - b). \quad (8)$$

By replacing \ddot{q}_u in (8) with (4), and substituting the expression of λ back to (1), we can get:

$$\begin{aligned} M^{-1}(\tau_m - \tau_{bias}) &= \\ M^{-1}G^T(GM^{-1}G^T)^{-1}(GM^{-1}(\tau_m - \tau_{bias}) - b) + \ddot{q} \end{aligned} \quad (9)$$

To simplify (9), we define the matrices and vector:

$$\begin{aligned} A(q, \pi_b) &= (I - G^{M+}G)M^{-1}, \\ c(q, \dot{q}, \ddot{q}, \pi_b) &= \ddot{q} + A\tau_{bias} - G^{M+}b, \end{aligned} \quad (10)$$

where I is an identity matrix and the motion variables and dynamic parameters of bones π_b in the parentheses show the dependency of A and c . (9) can be then rearranged into:

$$A(q, \pi_b)\tau_m = c(q, \dot{q}, \ddot{q}, \pi_b), \quad (11)$$

where it is worth mentioning that A transforms the muscle joint torque τ_m to a joint acceleration to leverage on the availability of the ground truth \ddot{q} in c for the loss calculation.

With the respective contribution of the superficial and deep muscles to τ_m , (11) can be expressed as:

$$A(J_{ms}^T(q)f_{ms}(q, \dot{q}, e_{ms}, \pi_{ms}) + J_{md}^T(q)f_{md}) = c, \quad (12)$$

where J_{ms} and f_{ms} are the muscle Jacobian and force vector of the superficial muscles. J_{ms} and J_{md} depend on the arm configuration q , which can be obtained from the measured arm movement, and f_{ms} can be computed based on a muscle model (introduced in III-F.1) with measured and preprocessed EMGs e_{ms} and the muscle model parameters π_{ms} . Therefore, the least-squares solution of the unknown deep muscle forces f_{md} can be calculated using the pseudoinverse $(\cdot)^+$ as:

$$f_{md} = (AJ_{md}^T)^+(\mathbf{c} - AJ_{ms}^T f_{ms}), \quad (13)$$

Based on (12) and (13), the parameter identification problem is formulated as an optimization problem with the loss function defined as follows:

$$l = \frac{\sum_{t=1}^T \|(I - AJ_{md}^T(AJ_{md}^T)^+)d_t(\pi_b, \pi_{ms})\|_2^2}{T \times \text{var}(d_t)}, \quad (14)$$

$$d = \mathbf{c} - AJ_{ms}^T f_{ms},$$

which is the normalized mean squared error due to the least-squares solution in (13). T represents the number of trajectory points in the dataset, and $\text{var}(d_t)$ denotes the variance of d_t with the initial guess of all the parameters. The model parameters to be identified in the optimization problem include ten dynamic parameters (mass, center of mass, and six parameters of the inertia matrix) for each of the *humerus*, *ulna*, and *radius* ($\pi_b \in \mathbb{R}^{30}$), and five parameters for each of the nine identifiable superficial muscles, and five other parameters common to all the muscles ($\pi_{ms} \in \mathbb{R}^{50}$), which will be introduced shortly in the following subsection.

F. Improving model realism

1) *Muscle contraction dynamics*: A musculotendon unit is modeled by a Hill-type model [47], in which a muscle is composed of an active contractile element in parallel to a passive elastic element, which is connected in series at a pennation angle (ϕ) to a tendon modeled as a passive elastic nonlinear spring. The force production of this system is governed by the muscle contraction dynamics, which converts the muscle activation a to the musculotendon force f_{mt} ² as:

$$f_{mt} = \cos(\phi)f_m^o(f^L(\tilde{l}_m)f^V(\tilde{v}_m)a + f^{PE}(\tilde{l}_m)), \quad (15)$$

$$f_{mt} = f_m^o(f^T(\tilde{l}_t)), \quad (16)$$

where both (15) and (16) can be used to calculate the force f_{mt} because of the force equilibrium between the muscle and the tendon [7]. f^L , f^V , f^{PE} , f^T are four generic, normalized, and time-invariant force curves for all the musculotendon units. Their inputs: the muscle length l_m , muscle velocity v_m , and tendon length l_t , are normalized by the optimal muscle fiber length ($\tilde{l}_m = l_m/l_m^o$), maximum muscle contraction velocity ($\tilde{v}_m = v_m/v_m^{max}$), and tendon slack length ($\tilde{l}_t = l_t/l_t^s$), respectively. Their outputs are normalized by the maximum muscle isometric force f_m^o . f_m^o , l_m^o , v_m^{max} , $\phi_o(\phi$ when $l_m = l_m^o)$, and l_t^s are the five

² f_{mt} represents each of the elements in the muscle force vector f_m in (1), the subscript t here indicates the fact that the muscle force is delivered to the bone through a tendon for causing a joint torque.

musculotendon-specific parameters to be identified for each of the nine identifiable superficial muscles.

In the MyoSuite model used in [17], the tendon is assumed to be rigid. Therefore, l_t^s does not exist, and the pennation angle is not modeled either. In addition, the four force curves are simplified in the MyoSuite model. However, l_t^s , ϕ_o , and the curves are very important for the force-generating behavior of a musculotendon unit [10], [11]. In OpenSim, quintic Bézier splines are used to model these curves, allowing for accurate fitting of the experimental data [48]. These splines are parametric equations where the parameter needs to be first calculated based on the input to be able to compute the corresponding output. An iterative numerical algorithm, such as the Newton-Raphson method used in OpenSim, is required to find the solution of the fifth-order polynomial equation for the parameter, which is slow when integrated into a large-scale differentiable optimization framework. To make the optimization more efficient, a differentiable piecewise function consisting of between 8 and 15 polynomials connected by optimized line segments is developed to fit each of the four OpenSim force curves. Since the polynomials directly express the relation between the input and output, they allow for efficient calculation of the derivative of the output with respect to the input as part of the chain of automatic differentiation. In the full differentiable optimization pipeline, (15) is first used to optimize the four muscle-related parameters, i.e., f_m^o , l_m^o , v_m^{max} , and ϕ_o , and when their good estimates are found (loss is low), (16) is then used to optimize l_t^s .

2) *Muscle activation dynamics*: As shown in Fig. 1, muscle activation dynamics is an upstream module with respect to the muscle contraction dynamics. It models how the neural excitations u generated by the alpha motor neurons can affect the activation level a of their innervated muscles as [7]:

$$\dot{a} = \frac{u - a}{t(u, a)} \quad (17)$$

$$t(u, a) = \begin{cases} t_{act}(0.5 + 1.5a) & u > a \\ t_{de}/(0.5 + 1.5a) & u \leq a \end{cases} \quad (18)$$

where t_{act} and t_{de} are the activation and deactivation time constants, which affect how fast the muscles are activated and deactivated by u . These two parameters are assumed to be the same for different muscles, which need to be identified in the optimization.

At each iteration during the optimization, when the parameters are updated, the time integration of (17) for getting the full profile of a is time-consuming when the number of time steps is large. Since $a, u \in [0, 1]$, it is guaranteed that $t > 0$, which ensures the solution of the exponentially decaying system (17) can converge to the excitation u over time. By leveraging the guaranteed convergence, the full trajectory is divided into smaller segments, which are all assumed to have an initial a of 0. An explicit Runge-Kutta method is used to solve for every segment of the trajectory in parallel to speed up the time integration. This would result in inaccurate activations at the beginning of each segment (except the

first one) due to the wrong initial guess, but the activations then quickly converge to the ground truth. The errors at the beginning of each segment are eliminated by redoing the time integration for the first few time steps of each segment, using the accurate final activation of the previous segment as the initial a in a second pass.

3) *EMG-to-excitation dynamics*: To capture the electro-mechanical time delay t_d from the onset of the EMG to the onset of the resulting muscle force production, an EMG-to-excitation dynamics [49] is used as an upstream module for the muscle activation dynamics. It converts the preprocessed EMG signals e to the neural excitation u , which is modeled by a recursive filter [49]:

$$u(t) = \alpha e(t - d) - \beta_1 u(t - 1) - \beta_2 u(t - 2), \quad (19)$$

where d is the time delay, α, β_1, β_2 are filter coefficients. To ensure the filter has unit gain and stability, the following relations must hold:

$$\begin{aligned} \alpha &= 1 + \beta_1 + \beta_2, \\ \beta_1 &= c_1 + c_2, \\ \beta_2 &= c_1 \cdot c_2, \\ |c_1|, |c_2| &< 1. \end{aligned} \quad (20)$$

c_1 , c_2 , and d are subject-specific [49] and are therefore considered learnable parameters common to all the muscles in our model. Directly making d learnable is not feasible, since it is a non-continuous index (an integer representing multiples of the sampling period) with respect to which the derivative of u doesn't exist. To solve this, we define the continuous time delay t_d as the learnable parameter, and design a differentiable function to map t_d to the continuous coefficients, γ and $1 - \gamma$, of the two neighboring time indices, d_l and d_h , as:

$$\begin{aligned} u(t) &= \alpha[\gamma e(t - d_l) + (1 - \gamma)e(t - d_h)] \\ &\quad - \beta_1 u(t - 1) - \beta_2 u(t - 2), \\ d_h &= \text{ceil}(t_d) \\ d_l &= \text{floor}(t_d) \\ \gamma &= (1 - t_d + d_l) \end{aligned} \quad (21)$$

IV. COMPARATIVE SIMULATIONS

To the best knowledge of the authors, there exists no method for parameter identification without the reconstruction of deep muscle EMGs (in the cases where the effect of the deep PM muscles cannot be ignored). To examine how well the model parameters can be estimated without deep muscle EMG reconstruction, our proposed method (M1) was compared against the simultaneous optimization method (M2), where all the muscle EMGs were assumed to be available (as the best possible case of deep muscle EMG reconstruction).

The loss calculation, initial conditions, and differentiable optimization pipeline of M1 and M2 are identical, except for the availability of deep muscle EMGs. The PyTorch automatic differentiation tool [42] was used to calculate the loss gradient and execute the differentiable optimization for both M1 and M2, and only the identifiable model parameters of M1 were used for the comparison between the two methods.

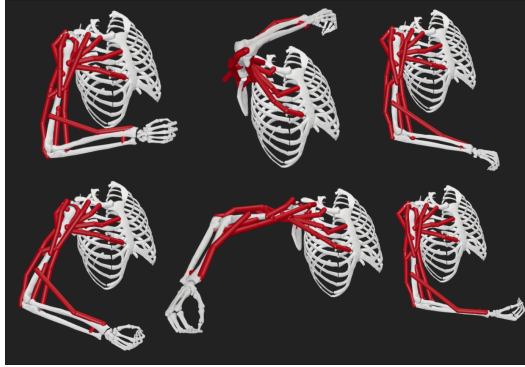


Fig. 3: Snapshots of the OpenSim arm configurations taken at three different times for each of two arm movements used in the training (each row represents one arm movement).

A. Comparison settings

Training datasets of two different arm movements were generated by driving the ground truth arm model in OpenSim through the forward dynamics with the neural excitations of all the muscles as the input calculated from the synthesized irregular EMG signals, shown in Fig. 1. The excitations of only the superficial muscles were fed into our differentiable arm model for the differentiable optimization in M1, while all the muscle excitations were provided in M2. At each time step, the collected data comprised joint positions, velocities, and accelerations, as well as the muscle lengths, velocities, and moment arms. Fig. 3 shows the snapshots taken at three different times for each of the two arm movements.

B. Evaluation criteria

Three criteria, Cr_1 , Cr_2 , and Cr_2^m , were used for the evaluation of the parameter estimation accuracy. Cr_1 describes how far a solution is from the ground truth:

$$Cr_1 = \frac{\|\hat{\pi} - \pi_{gt}\|_2}{\|\pi_{gt}\|_2} \times 100\%, \quad (22)$$

and Cr_2 is the mean of the percentage errors of all the estimated parameters, eliminating the effect of different units:

$$Cr_2 = \frac{1}{n} \sum_{i=1}^n \frac{|\hat{\pi}_i - \pi_{gti}|}{|\pi_{gti}|} \times 100\%, \quad (23)$$

and Cr_2^m refers to the mean of the percentage errors of only estimated muscle parameters.

C. Results

For each of the two arm movements, five sets of initial guesses for the learnable parameters were sampled from the normal distribution and used for each of the two methods.

$$\pi_0 \sim N(\pi_{gt}, 0.1\pi_{gt}), \quad (24)$$

Each of the total 20 simulation runs was conducted for 10K epochs, followed by an additional 2K epochs to optimize the tendon slack length based on the other optimized parameters. All the simulations were completed on a workstation with an Intel Core I9-14900KS CPU and 64GB of memory. The computation time per epoch was about 0.77s, yielding a

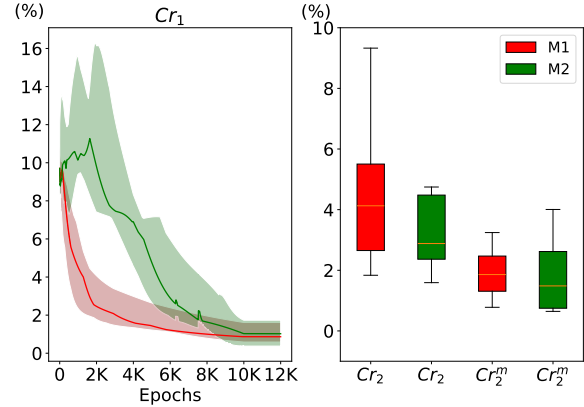


Fig. 4: Distance error curves in percentage (Cr_1) of 10 runs over 12K iterations of M1: differential optimization without deep muscle EMGs and M2: differential optimization with deep muscle EMGs. The solid line denotes the median, while the upper and lower boundaries of the shaded area represent upper and lower quartiles, respectively (left). Boxplots of final parameter estimate mean error Cr_2 and final muscle parameter mean error Cr_2^m (right).

total runtime of about 2.5 hours for each run. The parameter estimation results of the comparative methods (M1 and M2) in terms of the three criteria are shown in Fig. 4 and Fig. 5.

In Fig. 4, it can be observed that our proposed method M1 converged faster than M2 in terms of Cr_1 . However, at the 10K epoch mark, the methods performed similarly in terms of all the criteria. With the final Cr_2 , the performance of M1 was slightly worse than M2, while M1 achieved at least comparable results at the end of the optimization with Cr_2^m . It seems to imply that, with more learnable parameters in M2, the optimization problem was harder to solve but had the potential to find a better solution. However, the estimates of all the identifiable parameters of superficial muscles were already as good as M2. This is important as the bone parameter uncertainty has less impact on the dynamic uncertainty than the kinematic parameter uncertainty, shown in [9], but the muscle parameters greatly influence force-generating behavior of the musculotendon system [10].

There exists redundancy in the bone dynamic parameters, i.e., an infinite number of parameter solutions can achieve the same dynamic behavior of bones. However, a set of dynamic coefficients, as linear combinations of the original dynamic parameters, can be uniquely identified [50]. These coefficients are a minimum set that can determine the dynamic behavior of bones. Therefore, the original 30 bone dynamic parameters were converted to a set of 17 dynamic coefficients using the approach in [51], and the convergence of these coefficients to their ground truth values can be seen in Fig. 5. It is clear that most parameters could be estimated decently well by both methods, and in most cases, parameters converged actually faster and more robustly with M1 compared to M2. However, some of the parameters, e.g. c_1, c_2, ϕ_o , seemed to converge more slowly than the others for both methods. It is worth noting that *BIClong* and *BICshort* are not pennated muscles, therefore, their ϕ_o could not be set to a value other than their ground truth value of zero, as shown in Fig. 5.

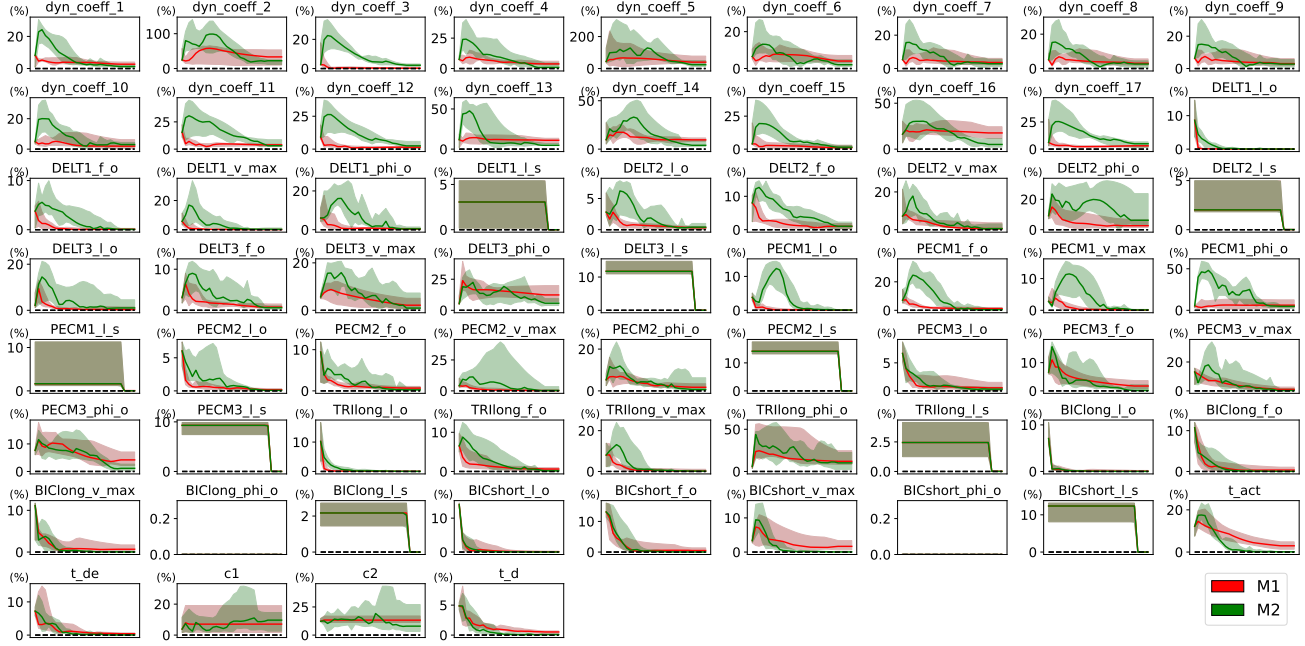


Fig. 5: Percentage errors of the parameter estimates over 12k epochs for both methods M1 (red, without deep muscle EMGs) and M2 (green, with deep muscle EMGs). The solid line and shaded area represent the median, upper and lower quartiles of the percentage error.

V. IMPLICATIONS

This simulation study is an important step for the practical use of the proposed parameter identification method with differentiable optimization, i.e., we considered the inaccessibility of the deep muscle activation and improved the realism of the musculoskeletal model, which simulates the real situation as much as possible. The anatomical features of the human arm (that is, moment arms of the deep muscles) were utilized to estimate the shoulder muscle/tendon parameters without deep muscle EMG reconstruction. It is valuable to accurately and invasively estimate the parameters of the shoulder-related muscles and tendons, as the shoulder typically needs to bear a large joint torque and is more prone to problems compared to other arm joints in physically demanding tasks. This method can enable, for instance, the convenient assessment of shoulder muscle strength and tendon stress-strain curve for many healthcare-related applications.

VI. CONCLUSIONS AND FUTURE WORK

In this work, we proposed to simultaneously identify the bone and muscle parameters of a subject-specific human arm musculoskeletal model without reconstruction of the deep muscle EMGs. This was achieved by treating the deep muscle behavior as a black box, and only using the best possible least-squares solution of the deep muscle forces to calculate the loss gradient with respect to the model parameters for optimizing the parameters within a framework of differentiable optimization. Satisfying results were observed in comparative simulations. Although a good initial guess of the model parameters can be obtained with appropriate scaling methods [10], [11] based on a template model, more simulation tests with larger initial parameter errors and real experiments will be carried out in the future.

REFERENCES

- C. Fang, L. Peternel, A. Seth, M. Sartori, K. Mombaur, and E. Yoshida, “Human modeling in physical human-robot interaction: A brief survey,” *IEEE Robotics and Automation Letters*, vol. 8, no. 9, pp. 5799–5806, 2023.
- A. Seth, J. L. Hicks, T. K. Uchida, A. Habib, C. L. Dembia, J. J. Dunne, C. F. Ong, M. S. DeMers, A. Rajagopal, M. Millard *et al.*, “OpenSim: Simulating musculoskeletal dynamics and neuromuscular control to study human and animal movement,” *PLoS computational biology*, vol. 14, no. 7, p. e1006223, 2018.
- H. Wang, V. Caggiano, G. Durandau, M. Sartori, and V. Kumar, “Myosim: Fast and physiologically realistic mujoco models for musculoskeletal and exoskeletal studies,” in *2022 International Conference on Robotics and Automation (ICRA)*. IEEE, 2022, pp. 8104–8111.
- L. Peternel, C. Fang, M. Laghi, A. Bicchi, N. Tsagarakis, and A. Ajoudani, “Human arm posture optimisation in bilateral teleoperation through interface reconfiguration,” in *2020 8th IEEE RAS/EMBS International Conference for Biomedical Robotics and Biomechatronics (BioRob)*. IEEE, 2020, pp. 1102–1108.
- S. Barbat-Artigas, Y. Rolland, M. Zamboni, and M. Aubertin-Leheudre, “How to assess functional status: a new muscle quality index,” *The Journal of nutrition, health and aging*, vol. 16, no. 1, pp. 67–77, 2012.
- W. Wu, P. V. Lee, A. L. Bryant, M. Galea, and D. C. Ackland, “Subject-specific musculoskeletal modeling in the evaluation of shoulder muscle and joint function,” *Journal of biomechanics*, vol. 49, no. 15, pp. 3626–3634, 2016.
- T. K. Uchida and S. L. Delp, *Biomechanics of movement: the science of sports, robotics, and rehabilitation*. Mit Press, 2021.
- M. S. Andersen, “Introduction to musculoskeletal modelling,” in *Computational modelling of biomechanics and biotribology in the musculoskeletal system*. Elsevier, 2021, pp. 41–80.
- A. Muller, C. Pontonnier, and G. Dumont, “Uncertainty propagation in multibody human model dynamics,” *Multibody System Dynamics*, vol. 40, no. 2, pp. 177–192, 2017.
- C. Winby, D. Lloyd, and T. Kirk, “Evaluation of different analytical methods for subject-specific scaling of musculotendon parameters,” *Journal of biomechanics*, vol. 41, no. 8, pp. 1682–1688, 2008.
- L. Modenese, E. Ceseracciu, M. Reggiani, and D. G. Lloyd, “Estimation of musculotendon parameters for scaled and subject specific musculoskeletal models using an optimization technique,” *Journal of biomechanics*, vol. 49, no. 2, pp. 141–148, 2016.
- M. Sartori, M. Reggiani, D. Farina, and D. G. Lloyd, “Emg-driven forward-dynamic estimation of muscle force and joint moment about

multiple degrees of freedom in the human lower extremity," *PloS one*, vol. 7, no. 12, p. e52618, 2012.

[13] A. Falisse, S. Van Rossum, I. Jonkers, and F. De Groot, "Emg-driven optimal estimation of subject-specific hill model muscle-tendon parameters of the knee joint actuators," *IEEE Transactions on Biomedical Engineering*, vol. 64, no. 9, pp. 2253–2262, 2016.

[14] G. Venture, K. Yamane, and Y. Nakamura, "Identifying musculo-tendon parameters of human body based on the musculo-skeletal dynamics computation and hill-stroeve muscle model," in *5th IEEE-RAS International Conference on Humanoid Robots, 2005*. IEEE, 2005, pp. 351–356.

[15] M. Hayashibe, G. Venture, K. Ayusawa, and Y. Nakamura, "Muscle strength and mass distribution identification toward subject-specific musculoskeletal modeling," in *2011 IEEE/RSJ International Conference on Intelligent Robots and Systems*. IEEE, 2011, pp. 3701–3707.

[16] G. Durandau, D. Farina, and M. Sartori, "Robust real-time musculoskeletal modeling driven by electromyograms," *IEEE transactions on biomedical engineering*, vol. 65, no. 3, pp. 556–564, 2017.

[17] Y. Zhou, P. Sanderink, S. J. Lemming, and C. Fang, "Diff-msm: Differentiable musculoskeletal model for simultaneous identification of human muscle and bone parameters," in *2025 IEEE/RSJ International Conference on Intelligent Robots and Systems (IROS)*. IEEE, 2025.

[18] A. Péter, E. Andersson, A. Hegyi, T. Finni, O. Tarassova, N. Cronin, H. Grundström, and A. Arndt, "Comparing surface and fine-wire electromyography activity of lower leg muscles at different walking speeds," *Frontiers in physiology*, vol. 10, p. 1283, 2019.

[19] M. Al-Ayyad, H. A. Owida, R. De Fazio, B. Al-Naami, and P. Visconti, "Electromyography monitoring systems in rehabilitation: A review of clinical applications, wearable devices and signal acquisition methodologies," *Electronics*, vol. 12, no. 7, p. 1520, 2023.

[20] D. A. Winter, *Biomechanics and motor control of human movement*. John wiley & sons, 2009.

[21] C. Fang, A. Ajoudani, A. Bicchi, and N. G. Tsagarakis, "A real-time identification and tracking method for the musculoskeletal model of human arm," in *2018 IEEE International Conference on Systems, Man, and Cybernetics (SMC)*. IEEE, 2018, pp. 3472–3479.

[22] W. L. Goffe, G. D. Ferrier, and J. Rogers, "Global optimization of statistical functions with simulated annealing," *Journal of econometrics*, vol. 60, no. 1-2, pp. 65–99, 1994.

[23] J. F. Schutte, B.-I. Koh, J. A. Reinbolt, R. T. Haftka, A. D. George, and B. J. Fregly, "Evaluation of a particle swarm algorithm for biomechanical optimization," 2005.

[24] G. Rao, D. Amarantini, E. Berton, and D. Favier, "Influence of body segments' parameters estimation models on inverse dynamics solutions during gait," *Journal of biomechanics*, vol. 39, no. 8, pp. 1531–1536, 2006.

[25] C. Pizzolato, D. G. Lloyd, M. Sartori, E. Ceseracciu, T. F. Besier, B. J. Fregly, and M. Reggiani, "Cenims: A toolbox to investigate the influence of different neural control solutions on the prediction of muscle excitation and joint moments during dynamic motor tasks," *Journal of biomechanics*, vol. 48, no. 14, pp. 3929–3936, 2015.

[26] K. M. Steele, M. C. Tresch, and E. J. Perreault, "The number and choice of muscles impact the results of muscle synergy analyses," *Frontiers in computational neuroscience*, vol. 7, p. 105, 2013.

[27] D. Ao and B. J. Fregly, "Comparison of synergy extrapolation and static optimization for estimating multiple unmeasured muscle activations during walking," *Journal of NeuroEngineering and Rehabilitation*, vol. 21, no. 1, p. 194, 2024.

[28] D. Ao, M. M. Vega, M. S. Shourijeh, C. Patten, and B. J. Fregly, "Emg-driven musculoskeletal model calibration with estimation of unmeasured muscle excitations via synergy extrapolation," *Frontiers in bioengineering and biotechnology*, vol. 10, p. 962959, 2022.

[29] M. Sartori, L. Gizzi, D. G. Lloyd, and D. Farina, "A musculoskeletal model of human locomotion driven by a low dimensional set of impulsive excitation primitives," *Frontiers in computational neuroscience*, vol. 7, p. 79, 2013.

[30] M. F. Rabbi, G. Davico, D. G. Lloyd, C. P. Carty, L. E. Diamond, and C. Pizzolato, "Muscle synergy-informed neuromusculoskeletal modelling to estimate knee contact forces in children with cerebral palsy," *Biomechanics and Modeling in Mechanobiology*, vol. 23, no. 3, pp. 1077–1090, 2024.

[31] N. Lambert-Shirzad and H. M. Van Der Loos, "On identifying kinematic and muscle synergies: a comparison of matrix factorization methods using experimental data from the healthy population," *Journal of neurophysiology*, vol. 117, no. 1, pp. 290–302, 2017.

[32] N. A. Turpin, S. Uriac, and G. Dalleau, "How to improve the muscle synergy analysis methodology?" *European journal of applied physiology*, vol. 121, no. 4, pp. 1009–1025, 2021.

[33] K. Taneja, X. He, Q. He, X. Zhao, Y.-A. Lin, K. J. Loh, and J.-S. Chen, "A feature-encoded physics-informed parameter identification neural network for musculoskeletal systems," *Journal of biomechanical engineering*, vol. 144, no. 12, p. 121006, 2022.

[34] J. Zhang, Y. Zhao, T. Bao, Z. Li, K. Qian, A. F. Frangi, S. Q. Xie, and Z.-Q. Zhang, "Boosting personalized musculoskeletal modeling with physics-informed knowledge transfer," *IEEE Transactions on Instrumentation and Measurement*, vol. 72, pp. 1–11, 2022.

[35] S. Ma, J. Zhang, C. Shi, P. Di, I. D. Robertson, and Z.-Q. Zhang, "Physics-informed deep learning for muscle force prediction with unlabeled semg signals," *IEEE Transactions on Neural Systems and Rehabilitation Engineering*, vol. 32, pp. 1246–1256, 2024.

[36] R. Kumar, T. Tripura, S. Chakraborty, and S. Roy, "Deep muscle electromyogram construction using a physics-integrated deep learning approach," *Engineering Applications of Artificial Intelligence*, vol. 159, p. 111613, 2023.

[37] M. Lutter, J. Silberbauer, J. Watson, and J. Peters, "Differentiable physics models for real-world offline model-based reinforcement learning," in *2021 IEEE International Conference on Robotics and Automation (ICRA)*. IEEE, 2021, pp. 4163–4170.

[38] E. Granados, A. Boulias, K. Bekris, and M. Aanjaneya, "Model identification and control of a low-cost mobile robot with omnidirectional wheels using differentiable physics," in *2022 International Conference on Robotics and Automation (ICRA)*. IEEE, 2022, pp. 1358–1364.

[39] K. Wang, W. R. Johnson, S. Lu, X. Huang, J. Booth, R. Kramer-Bottiglio, M. Aanjaneya, and K. Bekris, "Real2sim2real transfer for control of cable-driven robots via a differentiable physics engine," in *2023 IEEE/RSJ International Conference on Intelligent Robots and Systems (IROS)*. IEEE, 2023, pp. 2534–2541.

[40] J. Degrave, M. Hermans, J. Dambre, and F. Wyffels, "A differentiable physics engine for deep learning in robotics," *Frontiers in neurorobotics*, vol. 13, p. 6, 2019.

[41] R. Newbury, J. Collins, K. He, J. Pan, I. Posner, D. Howard, and A. Cosgun, "A review of differentiable simulators," *IEEE Access*, 2024.

[42] A. Paszke, S. Gross, S. Chintala, G. Chanan, E. Yang, Z. DeVito, Z. Lin, A. Desmaison, L. Antiga, and A. Lerer, "Automatic differentiation in pytorch," 2017.

[43] K. R. Saul, X. Hu, C. M. Goehler, M. E. Vidt, M. Daly, A. Velisar, and W. M. Murray, "Benchmarking of dynamic simulation predictions in two software platforms using an upper limb musculoskeletal model," *Computer methods in biomechanics and biomedical engineering*, vol. 18, no. 13, pp. 1445–1458, 2015.

[44] E. N. Marieb and K. Hoehn, *Human anatomy & physiology*. Pearson education, 2007.

[45] M. A. Sherman, A. Seth, and S. L. Delp, "Simbody: multibody dynamics for biomedical research," *Procedia Iutam*, vol. 2, pp. 241–261, 2011.

[46] C. Fang, A. Ajoudani, A. Bicchi, and N. G. Tsagarakis, "Online model based estimation of complete joint stiffness of human arm," *IEEE Robotics and Automation Letters*, vol. 3, no. 1, pp. 84–91, 2017.

[47] F. E. Zajac, "Muscle and tendon: properties, models, scaling, and application to biomechanics and motor control," *Critical reviews in biomedical engineering*, vol. 17, no. 4, pp. 359–411, 1989.

[48] M. Millard, T. Uchida, A. Seth, and S. L. Delp, "Flexing computational muscle: modeling and simulation of musculotendon dynamics," *Journal of biomechanical engineering*, vol. 135, no. 2, p. 021005, 2013.

[49] D. G. Lloyd and T. F. Besier, "An emg-driven musculoskeletal model to estimate muscle forces and knee joint moments in vivo," *Journal of biomechanics*, vol. 36, no. 6, pp. 765–776, 2003.

[50] C. Gaz, M. Cognetti, A. Oliva, P. R. Giordano, and A. De Luca, "Dynamic identification of the franka emika panda robot with retrieval of feasible parameters using penalty-based optimization," *IEEE Robotics and Automation Letters*, vol. 4, no. 4, pp. 4147–4154, 2019.

[51] C. G. Atkeson, C. H. An, and J. M. Hollerbach, "Estimation of inertial parameters of manipulator loads and links," *The International Journal of Robotics Research*, vol. 5, no. 3, pp. 101–119, 1986.